XRay Spectroscopy

James Amarel and Kevin Pederson

March 17, 2017

1 Results and Analysis

A 100 mCi ^{241}Am source irradiates our material sample with low energy gamma rays, causing the sample to be either photoionized or undergo internal conversion, where both processes result in the emission of x-rays. We use a temperature regulated silicon drift detector to create a voltage pulse of height proportional to the sample emitted radiation energy, which is binned into channels by a multi channel analyzer (MCA) to form a histogram of the ray counts vs the MCA channel, where the channels are proportionally related to the x-ray energy and any sharp peaks, termed photopeaks, give a measurement of the incoming radiation energy. First, we measured the channel distance between iron's K_α and K_β transitions, as seen in Figure 1, to be 8.48 channels, and this value is proportional to the energy difference $\Delta E = 0.661$ keV between the lines, yielding a ratio of ≈80 eV per channel. Where a K x-ray means that an electron has transitioned into the $n = 1$ state, an α subscript means the transition electron originated in the $n = 2$ state, and a β subscript means the electron originated in the $n = 3$ state.

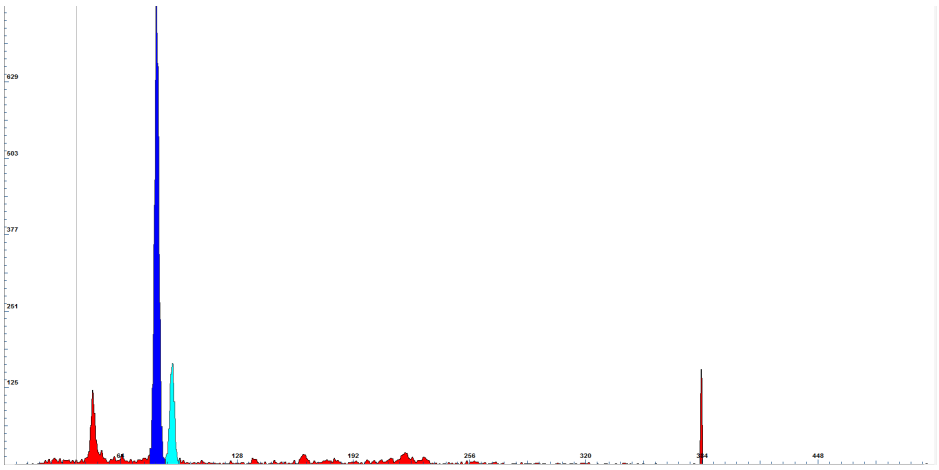

Figure 1: Iron x-ray spectra. The two photopeaks are highlighted in blue, the leftmost peak is later identified as background radiation, and the rightmost peak is due to our detector lumping all radiation of greater than 10 keV into the final bin.

To determine the resolution of our apparatus, we measured the full width half max of iron's K_α line to be 2.737 channels, which can be converted to ≈210 eV and is in agreement with the manufacturer specification of 200 ev. Then, we create a calibration equation relating the channel number to the x-ray energy, seen in Figure 2,

by recording the peak channels of the K_α and k_β lines of Cu, Ni, Zn, Zr, Mo, and Rh, where we determined the energies for this measurement (and all subsequent transition energies) from the X-Ray Data Booklet from the Berkeley National Lab [1].

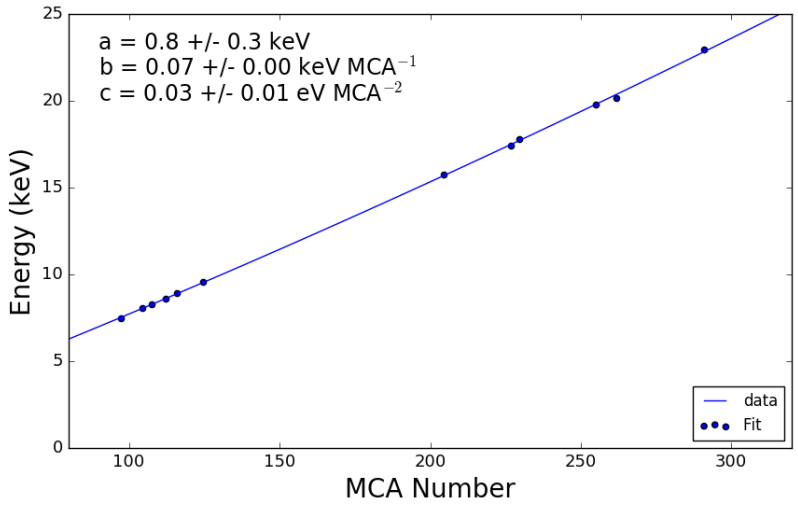

Figure 2: Results of the MCA calibration.

Next, we took a 200 s background spectra, shown in Figure 3, where we identify photopeaks of background radiation at channel numbers 48.09, 112.13, 137.09, and 164.08, where the software provides precision beyond a single channel by calculating the centroid of each peak. Peaks in these locations are present in many of the following results, note that we must consider the rate of background radiation when selecting the characteristic photopeaks of our samples.

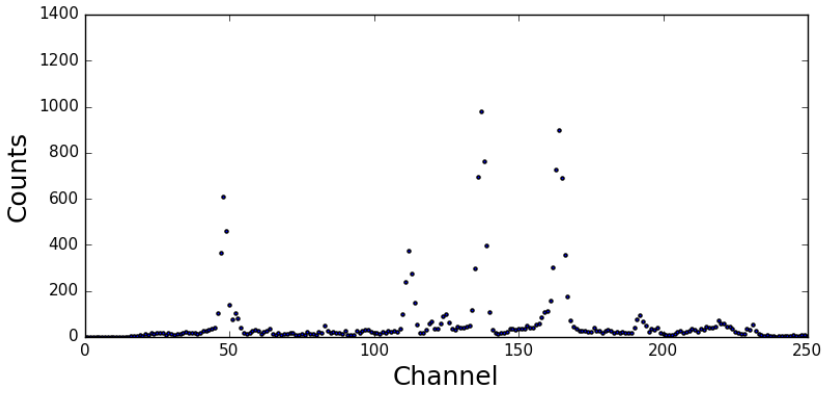

Figure 3: Background x-ray spectra. Rendered in alternate software for increased detail.

1.1 Moseley's Law

Moseley's law is an empirical law to show that the energy of atomic x-rays varies according to the atomic number Z. This relationship holds in the Bohr model of hydrogen

like atoms for the energy E of state n

$$E_n = -13.6Z^2/n^2 \text{eV} \tag{1}$$

where Z is the atomic number. Thus, the change in energy for any transition between hydrogen like states is proportional to the square of the atomic number. This concept can be extended to treat multi-electron atoms through the introduction of screened charge, by taking $Z \to Z - b$, where b is a constant factor to account for the apparent reduction in nuclear charge. Then, the x-ray energy is empirically determined as

$$E = a^2(Z-b)^2 \text{ and } E^{1/2} = a(Z-b) \tag{2}$$

where a is another empirical factor, along with b.

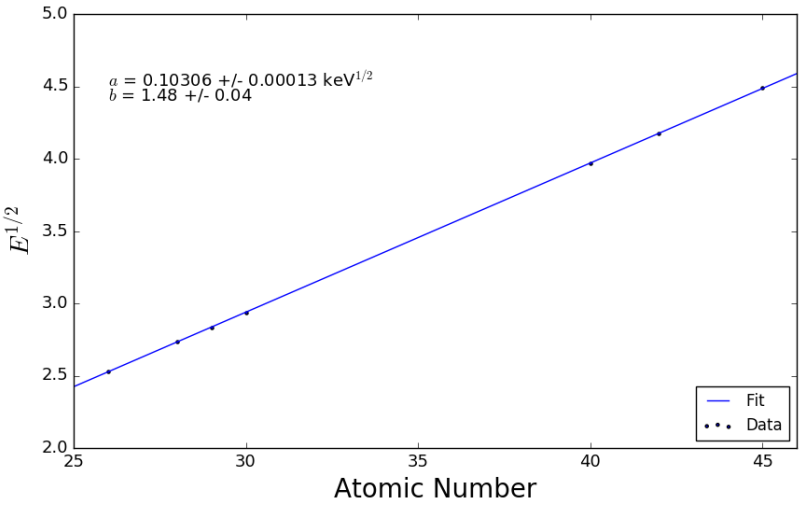

Figure 4: Linear least squares fit to Moseley's law.

From our table values of the K_{alpha} lines for Fe, Cu, Ni, Zn, Zr, Mo, and Rh, with their respective atomic numbers, we performed a linear least squares fit with Equation 2 to determine parameters $a = 0.10306 \pm 0.00013$ keV$^{1/2}$ and $b = 1.48 \pm 0.04$, shown in Figure 4. This calculation is more than ten standard deviations from Moseley's prediction of $a = 0.0101$ keV$^{1/2}$, but is in agreement with Moseley's prediction that b should be approximately 1. A measurement of $b > 1$ suggests that most of the shielding is determined by the electron that is already in the same atomic state as the hole, but the other electrons also form a sizable contribution as a hole.

We will now analyze the x-ray spectra of a wide range of materials, and use our calibration relation measurements of the x-ray energy to gain information about which transition the element undergoes, and then infer the composition of materials from the characteristic spectra of their constituents.

1.2 Tin

Figure 5 shows the MCA display of tin's x-ray spectra when under the effects of the radioactive ^{241}Am source. We eliminate all peaks except for the two highlighted on the right, as the three left sided peaks are background radiation, and the right edge peak

is detector induced. These photopeaks and their corresponding energies are listed in Table 1, which also contains our identification of the atomic transition. We selected the $K_{\alpha 1}$ and $K_{\beta 1}$ lines based on the closest listed match in the data chart, which are within one standard deviation of both our choices. Where the additional number subscript 1 indicates the highest energy of that that transition, which originates with $j = 3/2$.

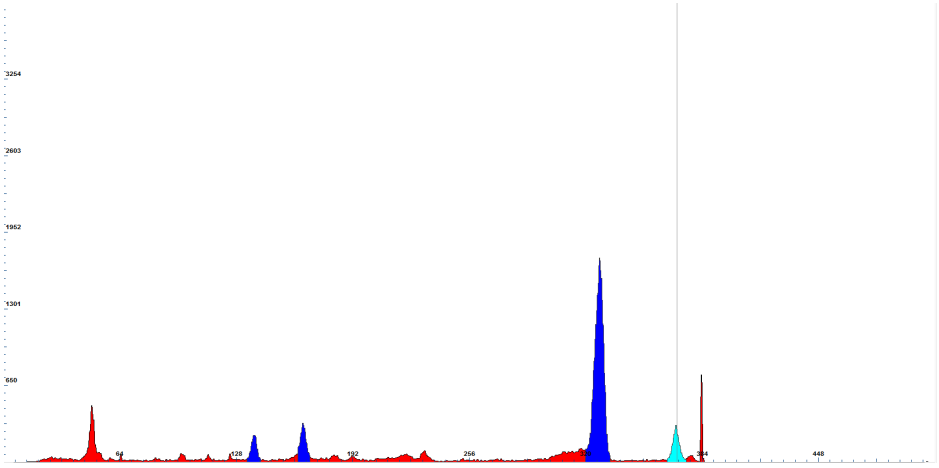

Figure 5: Tin x-ray spectra.

Table 1: Tin photopeak channel, corresponding gamma ray energy, predicted transition line, and the accepted table value for the energy of the transition line.

Channel	E_{meas} [keV]	Transition	E_{table} [keV]
326.71	25 ± 2	$K_{\alpha 1}$	25.3
369.09	29 ± 2	$K_{\beta 1}$	28.5

1.3 Lead

Figure 6 shows lead's x-ray spectra which contains the most photopeaks of all our samples. We eliminate all peaks except for those listed in Table 6 due to them being background noise. The remaining peaks and their corresponding energies are also listed in Table 2, where we have identified three of the photopeaks as transitions from our x-ray energy table to within one standard deviation. We now introduce the subscript 2 to our transition notation, which corresponds to an original state of $j = 1/2$. The three peaks labeled internal conversion are all patterned adjacent to a larger peak, and their cause is due to when an excited nucleus decays to a lower energy state by ejecting an inner electron. The ejected electron carries energy equal to the transition energy minus its binding energy.

So on the chance that a gamma ray excites an atom, as opposed to photoionizing it, the atom can decay to release an electron of slightly less energy than the incoming ray, which can create holes in other atoms. Thus, there is a main photopeak for photoionization paired with an edge that corresponds to the internal conversion scenario. Lead has the richest spectrum of well defined photopeaks, it is also the densest and carries the largest atomic number, both of which could generate more possible electronic transitions.

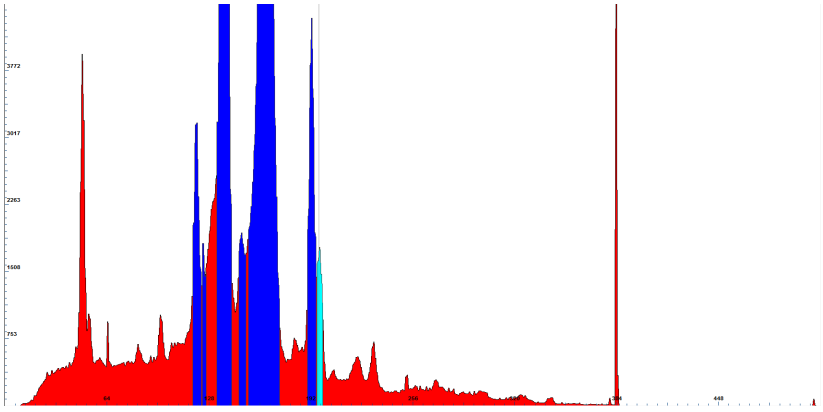

Figure 6: Lead x-ray spectra.

Table 2: Lead photopeak channel, corresponding gamma ray energy, predicted transition line next to the transition element, and the accepted table value for the energy of the transition line.

Channel	E_{meas} [keV]	Transition	E_{table} [keV]
119.8	9.17 ± 0.6	L_l	9.18
123.5	9.4 ± 0.9	Internal Conversion	
143.1	10.9 ± 0.6	Internal Conversion	
148.2	11.3 ± 0.6	$L_{\alpha 2}$	10.4
191.7	14.7 ± 0.7	$L_{\gamma 1}$	14.76
196.5	15.1 ± 0.9	Internal Conversion	

1.4 Brass

Figure 7 shows the x-ray spectra of brass, which only contains the two photopeaks listed in Table 3. Note that photopeak at channel 112 also appears in the background measurement, but when brass is present this peak rises at a much faster rate, so it isn't noise. Our photopeak identification is the $K_{\alpha 1}$ lines of copper and zinc, with both choices being within one standard deviation of our measurement, and in agreement with the fact that brass is metal alloy of mainly copper and zinc. It appears as if the composite nature of this alloy has removed the presence of the K_β lines that we observed when doing our calibration. Brass can be made from many different Copper to Zinc ratios, but as our two photopeaks are on the same order of magnitude, we can reasonably assume that the two elements are present in approximately similar quantities.

Table 3: Brass photopeak channel, corresponding gamma ray energy, predicted transition line with the transition element, and the accepted table value for the energy of the transition line.

Channel	E_{meas} [keV]	Transition	E_{table} [keV]
104.6	8.06 ± 0.6	Cu $K_{\alpha 1}$	8.04
112.9	8.66 ± 0.6	Zn $K_{\alpha 1}$	8.63

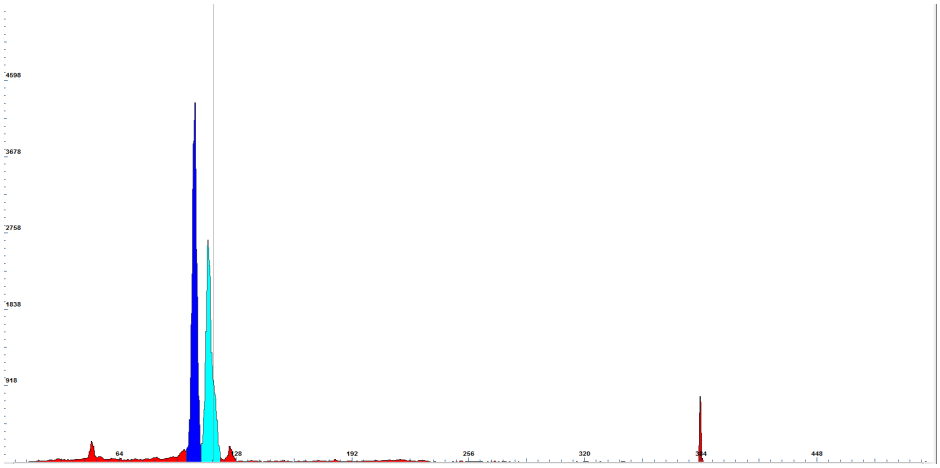

Figure 7: Brass x-ray spectra.

1.5 Stainless Steel

Figure 8 shows the x-ray spectra of steel, which we find contains the six photopeaks listed in Table 4. Many of the peaks are quite small, but not present in the background measurements, so we choose to include them, although more data would be desired before certain claims can be made. Our photopeak identification for steel's spectra includes K_α and K_β lines of chromium, iron, and nickel, with all choices being within one standard deviation of our measurement, and in agreement with the fact that steel is metal alloy of mainly chromium, iron, and nickel. In contrast with the case of Brass, the alloy nature of steel does not seem to restrict the available transitions of its elements. Stainless steel is predominantly iron, evidenced by the fact that the iron photopeaks are the largest. Then iron contains approximately 10% chromium and 2% nickel, both of which are present in Figure 8, but at an intensity lesser than iron's radiation.

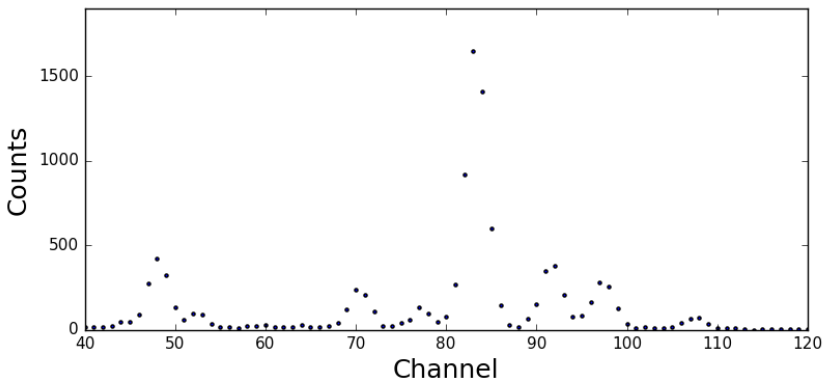

Figure 8: Stainless steel x-ray spectra. Rendered in an alternate program for increased detail.

1.6 Galvanized Steel

Figure 9 shows the x-ray spectra of galvanized steel, which is steel that has been submerged in a bath of molten metal in order to form a protective coating. We

Table 4: Stainless Steel photopeak channel, corresponding gamma ray energy, predicted transition line with transition element, and the accepted table value for the energy of the transition line. Note that the nickel lines are unresolved blends, so have been listed without a numerical subscript.

Channel	E_{meas} [keV]	Transition	E_{table} [keV]
70.36	5.6 ± 0.5	Cr $K_{\alpha 2}$	5.41
77.37	6.1 ± 0.5	Cr $K_{\beta 1}$	5.95
83.29	6.5 ± 0.5	Fe $K_{\alpha 1}$	6.4
91.61	6.4 ± 0.5	Fe $K_{\alpha 2}$	6.39
97.43	7.5 ± 0.6	Ni K_{α}	7.47
109	8.4 ± 0.6	Ni K_{β}	8.26

measured three photopeaks, listed in Table 5, which we believe to be due to iron and zinc transitions. The transitions listed are all within one standard deviation of our measurements, allowing us to identify the protective coating as being zinc, since zinc is not present in the stainless steel measurements. Also notice that the zinc coating seems to have reduced many of the peaks identified as being characteristic of steel to background levels.

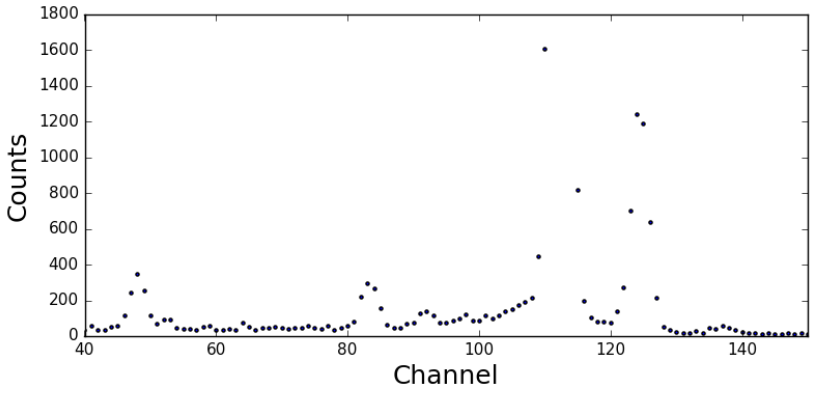

Figure 9: Galvanized steel x-ray spectra.

Table 5: Galvanized steel photopeak channel, corresponding gamma ray energy, predicted transition line with transition element, and the accepted table value for the energy of the transition line.

Channel	E_{meas} [keV]	Transition	E_{table} [keV]
83	6.5 ± 0.5	Fe $K_{\alpha 1}$	6.4
112.27	8.62 ± 0.6	Zn K_{α}	8.63
124.47	9.52 ± 0.6	Zn K_{β}	9.57

1.7 Unknown K1

Figure 10 shows the x-ray spectra of our first unknown material that we will identify. There are three peaks above background levels listed in Table 10, which we believe to be the characteristic lines of platinum. These are now labeled L x-rays, since they are

transitions into the n = 2 quantum state. This is because the atomic number of 78 for platinum means that the binding energy of its innermost electrons is greater than the 24.7 keV energy of the incoming gamma radiation, but the gamma carries enough energy to knock out electrons from the second shell. We decided on platinum as the best fit for this spectra because our measurements of the transition energy are well within one standard deviation of the accepted transition energies for platinum and it was the only single element that could match this spectrum.

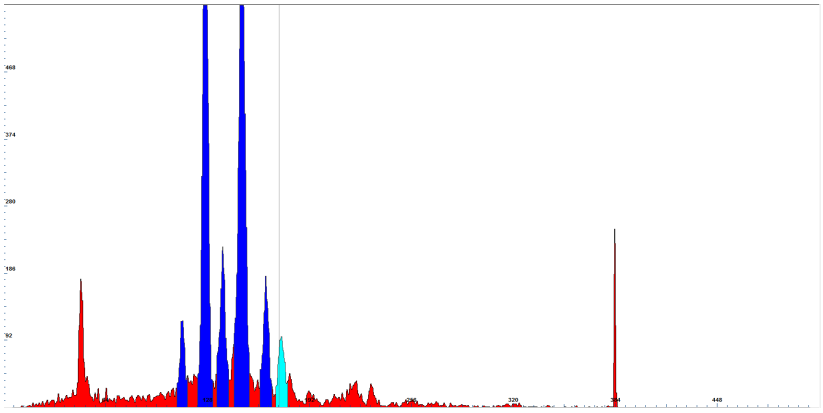

Figure 10: Unknown K1 x-ray spectra.

Table 6: Unknown 1 photopeak channel, corresponding gamma ray energy, predicted transition line, and the accepted table value for the energy of the transition line.

Channel	E_{meas} [keV]	Transition	E_{table} [keV]
126.17	9.7 ± 0.6	Pt L_{α}	9.4
149.14	11.4 ± 0.7	Pt $L_{\beta 2}$	11.25
173.88	13.3 ± 0.8	Pt $L_{\alpha 2}$	12.95

1.8 Unknown K2

Figure 11 shows the x-ray spectra of our second unknown, which we found to have only a single photopeak, listed in Table 5, that appears characteristic of silver. This choice for the accepted transition is within one standard deviation of our measurement. A single line makes this a weak measurement, since there are five elements (including silver) which have a K x-ray line within one standard deviation of our measured transition energy.

Table 7: Unknown 2 photopeak channel, corresponding gamma ray energy, predicted transition line, and the accepted table value for the energy of the transition line.

Channel	E_{meas} [keV]	Transition	E_{table} [keV]
286.66	22.46 ± 1.4	Ag K_{α}	22.1

1.9 Penny

Figure 12 shows the x-ray spectra of a coin penny, which we found to have two photopeaks, as shown in Table 8, that are the K_{α} lines of copper and zinc. These choices

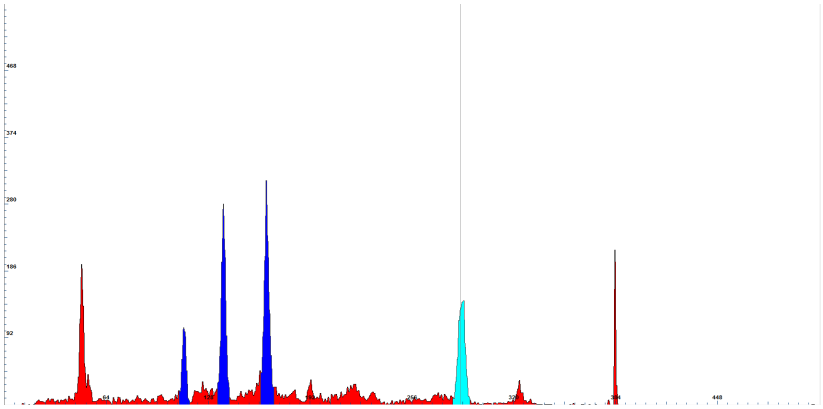

Figure 11: Unknown K2 x-ray spectra.

are within one standard deviation of our measurements and in agreement with the fact that a penny is made of copper and zinc. Interestingly, even though a penny is 5% zinc and 95% copper, the Cu and Zn photopeaks appear in similar magnitude, which is likely due to the fact that the penny is coated in zinc, so zinc absorbs more of the incoming gamma radiation and thus emits more x-rays.

Figure 12: Penny x-ray spectra.

Table 8: Penny photopeak channel, corresponding gamma ray energy, predicted transition line, and the accepted table value for the energy of the transition line.

Channel	E_{meas} [keV]	Transition	E_{table} [keV]
104.57	8.05 ± 0.6	Cu K_α	8.04
112.62	8.64 ± 0.6	Zn K_α	8.63

1.10 Quarter

Figure 13 shows the x-ray spectra of a coin quarter, which we found to have two photopeaks, as shown in Table 9, that are the K_α lines of copper and nickel. These choices are within one standard deviation of our measurements and in agreement with the fact that a quarter is made of copper and nickel. Again we see that despite the

fact that the quarter is only 8.33% nickel, the photopeaks of each element are similar in height.

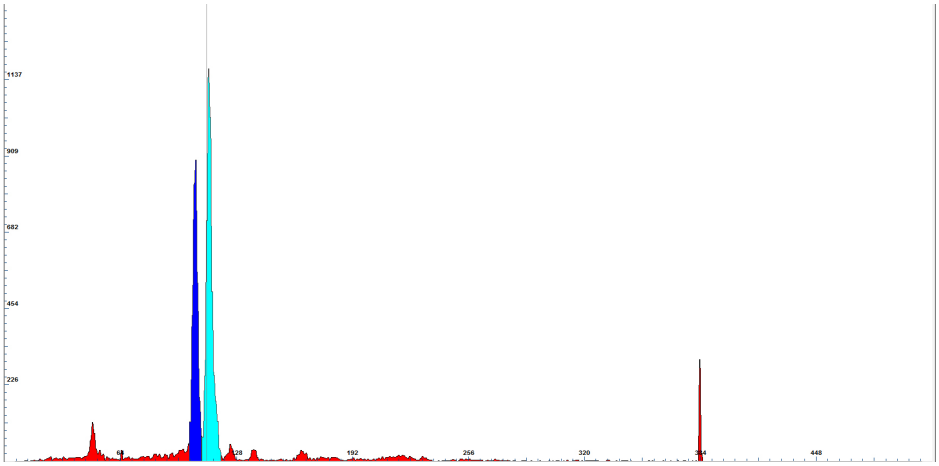

Figure 13: Quarter x-ray spectra.

Table 9: Quarter photopeak channel, corresponding gamma ray energy, predicted transition line, and the accepted table value for the energy of the transition line.

Channel	E_{meas} [keV]	Transition	E_{table} [keV]
97.39	7.52 ± 0.6	Ni K_α	7.47
104.72	8.06 ± 0.6	Cu K_α	8.04

1.11 Silver

Figure 14 shows the K_α and K_β photopeaks of a silver. The energies and transitions are shown in Table 10, where these choices are within one standard deviation of the accepted values.

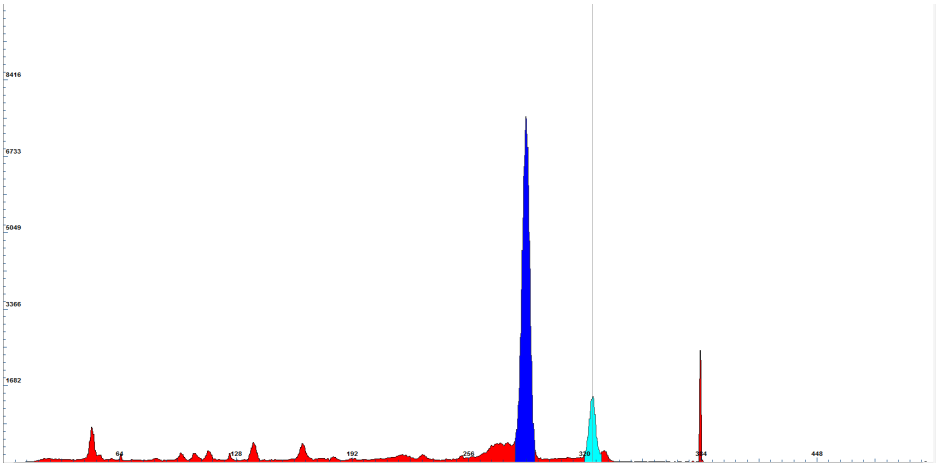

Figure 14: Silver x-ray spectra.

In our earlier identification of an unknown as silver, we did not witness a K_β line, but in this case we have measured a small peak at that location. It is possible that

Table 10: Silver photopeak channel, corresponding gamma ray energy, predicted transition line, and the accepted table value for the energy of the transition line.

Channel	E_{meas} [keV]	Transition	E_{table} [keV]
286.9	22.48 ± 1.4	K_α	22.08
323.6	25.65 ± 1.7	K_β	25.2

the coating on our unknown sample removed our ability to detect this peak, and now since we are using uncoated jewelry, it is now visible.

2 Conclusion

As we have seen time and again, the quantum mechanical nature of atoms gives rise to a finite set of allowed states, which gives each system characteristic transition lines. Our measurements indicate that as the material composition increases in complexity, so does its x-ray spectra, evidenced by the fact that our densest material, lead, has the richest decay schemes and composite materials can lose their tendency for certain transitions. Additionally, we identified internal conversion peaks that were only present in lead.

Furthermore, we discovered the composition of alloys brass, stainless steel, and galvanized steel by identifying the photopeaks of these samples and matching them to the characteristic lines of their constituent elements and from these measurements we infer some information about the relative quantities of each element in the alloy. For samples that were coated, we suspect that our low energy gamma radiation does not travel deep into the thin coatings, because coated materials displayed fewer photopeaks than their corresponding uncoated counterparts. Additionally, the coating created a peak of approximately the same size as the main element, even though the coating was present in a much smaller quantity.

References

[1] X-RAY DATA BOOKLET, 2009. URL `http://xdb.lbl.gov/`.